Effects of Mean Flow Direction on Energy, Isotropy, and Coherence of Baroclinically Unstable Beta-Plane Geostrophic Turbulence

BRIAN K. ARBIC*

MIT/WHOI Joint Program in Oceanography, Massachusetts Institute of Technology, Cambridge, and Woods Hole Oceanographic Institution, Woods Hole, Massachusetts

GLENN R. FLIERL

Program in Atmospheres, Oceans, and Climate, Department of Earth and Planetary Sciences, Massachusetts Institute of Technology, Cambridge, Massachusetts

(Manuscript received 15 March 2002, in final form 23 May 2003)

ABSTRACT

The effects of mean flow direction on statistically steady, baroclinically unstable, beta-plane quasigeostrophic (QG) turbulence are examined in a two-layer numerical model. The turbulence is forced by an imposed, horizontally homogeneous, vertically sheared mean flow and dissipated by bottom Ekman friction. The model is meant to be an idealization of the midocean eddy field, which generally has kinetic energies larger than the mean and is isotropic. Energetic eddies can be generated even when planetary beta (β) dominates gradients of mean potential vorticity (PV; also, q), as long as the mean shear has a substantial meridional component. However, eddies are isotropic only when the angle between layer mean PV gradients exceeds approximately 90°. This occurs when planetary and shear-induced gradients are comparable. Maps of PV indicate that these gradients may indeed be comparable over much of the midocean. Coherent jets form when the mean flow has a substantial meridional component and β is large. When β is nonzero, but small enough to permit isotropy, and the zonal component of the mean flow is not strongly eastward, lattices of like-signed coherent vortices develop. Like-signed vortex formation from initial and forcing conditions without a vorticity preference has not been observed before in QG systems. The vortex arrays are sensitive to the details of small-scale dissipation. Both cyclonic and anticyclonic fields arise in the simulations, depending on initial conditions, but they have different energies, consistent with broken symmetries in the governing equations.

1. Introduction

In midocean gyres, time-varying geostrophic motions such as Rossby waves, coherent rings, and mesoscale eddies have kinetic energies exceeding that of mean flows by a factor of 50 or so (Gill et al. 1974; Wunsch 2001). The source of midocean mesoscale eddy energy is a matter of ongoing research. The Gulf Stream and other boundary currents generate rings and Rossby waves that advect and radiate into the interior (Richardson 1983; Chester et al. 1994). Other potential generation mechanisms include direct generation by winds (Frankignoul and Müller 1979; Müller and Frankignoul 1981) and baroclinic instability of midocean gyre flows (Orlanski and Cox 1973; Gill et al. 1974; Robinson and McWilliams 1974). Arbic (2000) has investigated the plausibility of local baroclinic instability as a generation mechanism. In the spirit of Larichev and Held (1995) and similar studies, the main tool is a statistically steady, two-layer, doubly periodic, quasigeostrophic (QG) numerical turbulence model forced by a horizontally homogeneous, vertically sheared mean flow and dissipated through bottom Ekman friction. The model is meant to represent a patch of the ocean gyre, large enough to contain many eddy lengths but small enough so that the mean flow varies slowly.

In a paper under review, we focus on the sensitivity of modeled eddy length scales and vertical structure to bottom friction. In Arbic and Flierl (2003) we examine the coherent vortices and spatial distributions of potential and kinetic energy in freely decaying and baroclinically unstable f-plane turbulence. In this paper, we study the effects of mean flow direction on beta-plane geostrophic turbulence. (Where the comparison is instructive, we will discuss f-plane results.) Planetary beta stabilizes zonal mean flows. However, midocean mean flows are inherently nonzonal. Linear analysis on a beta plane (Lorenz 1972; Robinson and McWilliams

* Current affiliation: Program in Atmospheric and Oceanic Sciences, Princeton University/GFDL, Princeton, New Jersey.

Corresponding author address: Brian K. Arbic, Program in Atmospheric and Oceanic Sciences, Princeton University/GFDL, P.O. Box CN710, Sayre Hall, Princeton, NJ 08544-0710.
E-mail: bka@gfdl.gov

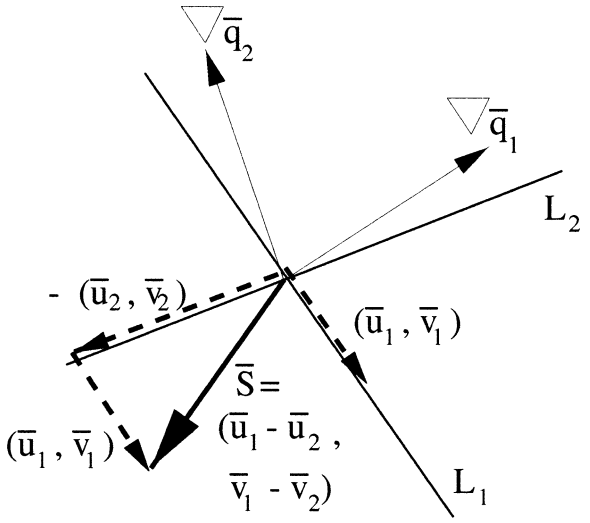

FIG. 1. Geometrical illustration of the procedure for choosing layer velocities. The lines L_1 and L_2 are perpendicular to the gradients of upper- and lower-layer mean PV, respectively. Velocity vectors lying along these lines as shown satisfy $J(\overline{\psi}, \overline{q}) = 0$ within each layer, while yielding the imposed shear vector **S**.

1974; Mak 1975; Rhines 1977; Mied 1978; Pedlosky 1987; Kamenkovich and Pedlosky 1996) indicates that nonzonal mean flows (and nonzonal flows in Rossby waves), no matter how weak, are nearly always unstable. Dubus (1999) and Spall (2000) examined the possibility that weak midocean currents with a substantial north–south component might produce energetic eddies. Their numerical experiments were fully nonlinear and forced by inhomogeneous mean flows—for instance, Spall's work was in a wind-driven gyre. We also perform fully nonlinear experiments, but with horizontally homogeneous mean flows. Since mean flow direction is fixed within each experiment, we can more easily isolate the effect of mean flow angle on eddy energy.

We document the dependence of eddy isotropy on the angle between layer mean potential vorticity (PV) gradients. This angle is a function of the relative strengths of planetary and shear-induced mean PV gradients, which we denote by P_S, as well as the direction of the mean shear. We also show that P_S and mean flow direction significantly impact coherent structure formation. Coherent features such as fronts, jets, and vortices are common in geophysical flows. In this paper we reserve the term ''coherent structures'' for structures that have tight, well-defined potential vorticity/streamfunction (q/ψ) relationships; in such cases, nonlinearity holds eddies together (Flierl et al. 1980). Two-dimensional structures having tight q/ψ relationships are an established part of inviscid theory (Stern 1975; Larichev and Reznik 1976) and of numerical simulations of freely decaying turbulence (McWilliams 1984; Montgomery et al. 1992). Flierl et al. (1980) generalized Stern's analytical modon solutions to stratified flow. Coherent vortices similar to those in McWilliams (1984) have been documented in simulations having stratification (cf. McWilliams et al. 1994) and in one-layer simulations with forcing and dissipation (cf. Maltrud and Vallis 1991). Other than Arbic and Flierl (2003) and the present work, we are not aware of any numerical or theoretical studies to date that have examined q/ψ relationships in flows having stratification, baroclinically unstable forcing, and dissipation present simultaneously, as happens in actual planetary flows.

2. Model and parameters

The governing equations are

$$\frac{\partial q_1}{\partial t} + \overline{u_1}\frac{\partial q_1}{\partial x} + \overline{v_1}\frac{\partial q_1}{\partial y} - \frac{\partial \overline{q_1}}{\partial x}\frac{\partial \psi_1}{\partial y} + \frac{\partial \overline{q_1}}{\partial y}\frac{\partial \psi_1}{\partial x} + J(\psi_1, q_1) = \text{ssd} \quad \text{and} \tag{1}$$

$$\frac{\partial q_2}{\partial t} + \overline{u_2}\frac{\partial q_2}{\partial x} + \overline{v_2}\frac{\partial q_2}{\partial y} - \frac{\partial \overline{q_2}}{\partial x}\frac{\partial \psi_2}{\partial y} + \frac{\partial \overline{q_2}}{\partial y}\frac{\partial \psi_2}{\partial x} + J(\psi_2, q_2) = -R_2\nabla^2\psi_2 + \text{ssd}, \tag{2}$$

where q (ψ) denotes potential vorticity (streamfunction), velocities are defined from the streamfunction in the usual way (cf. Pedlosky 1987), the Jacobian is defined by $J(A, B) = \partial A/\partial x\, \partial B/\partial y - \partial A/\partial y\, \partial B/\partial x$, overbars denote imposed time-mean quantities, subscripts 1 and 2 denote upper and lower layers, respectively, u (v) denotes zonal (meridional) velocity, R_2 is the Ekman decay rate, and ssd stands for small-scale dissipation. Fluctuation quantities do not have overbars and are defined as deviations from the mean. We set the ratio $\delta = H_1/H_2$ of upper to lower layer depths to 0.2, consistent with the surface-intensified stratification typical of midlatitudes (Fu and Flierl 1980). Fluctuation potential vorticities are

$$q_1 = \nabla^2\psi_1 + \frac{(\psi_2 - \psi_1)}{(1 + \delta)L_d^2} \quad \text{and}$$

$$q_2 = \nabla^2\psi_2 + \frac{\delta(\psi_1 - \psi_2)}{(1 + \delta)L_d^2}, \tag{3}$$

while mean PV gradients are

$$\frac{\partial \overline{q_1}}{\partial x} = \frac{(\overline{v_2} - \overline{v_1})}{(1 + \delta)L_d^2}, \qquad \frac{\partial \overline{q_2}}{\partial x} = \frac{\delta(\overline{v_1} - \overline{v_2})}{(1 + \delta)L_d^2},$$

$$\frac{\partial \overline{q_1}}{\partial y} = \beta + \frac{(\overline{u_1} - \overline{u_2})}{(1 + \delta)L_d^2}, \quad \text{and}$$

$$\frac{\partial \overline{q_2}}{\partial y} = \beta + \frac{\delta(\overline{u_2} - \overline{u_1})}{(1 + \delta)L_d^2}, \tag{4}$$

where L_d is the baroclinic deformation radius. Large β stabilizes zonal mean flows by preventing meridional PV gradients from changing sign between layers (Charney and Stern 1962). Nonzonal mean flows are more unstable because they create zonal gradients that change

sign independent of β. The cross product of layer mean PV gradients is

$$\nabla\overline{q_1} \times \nabla\overline{q_2} = -\frac{\beta(\overline{v_1} - \overline{v_2})}{L_d^2}\mathbf{k}, \tag{5}$$

where $\mathbf{k}$ is the unit vector in the vertical direction. On the f plane the angle between layer mean PV gradients is 180°, and for zonal flows on a beta plane the angle is either 0° or 180°, depending on flow criticality. The angle can take on values other than 0° or 180° if and only if β is nonzero and the mean flow is nonzonal.

The governing equations are most easily derived by assuming that $J(\overline{\psi}, \overline{q}) = 0$ and performing a Reynolds decomposition; otherwise one must make special assumptions about the forcing and dissipation (Arbic 2000). If we impose the shear vector ($\overline{u_1} - \overline{u_2}$, $\overline{v_1} - \overline{v_2}$), $J(\overline{\psi}, \overline{q}) = 0$ is satisfied in both layers if the mean velocities are equal to

$$\overline{u_1} = \beta L_d^2 + \frac{1}{1+\delta}(\overline{u_1} - \overline{u_2}),$$

$$\overline{u_2} = \beta L_d^2 - \frac{\delta}{1+\delta}(\overline{u_1} - \overline{u_2}),$$

$$\overline{v_1} = \frac{1}{1+\delta}(\overline{v_1} - \overline{v_2}), \quad \text{and} \quad \overline{v_2} = -\frac{\delta}{1+\delta}(\overline{v_1} - \overline{v_2}). \tag{6}$$

A geometric interpretation is given in Fig. 1. All of the nonzonal experiments shown in this paper satisfy (6). We have performed a few nonzonal experiments with the same magnitude of shear but in which $J(\overline{\psi}, \overline{q}) = 0$ is not satisfied. No differences were found in the results, indicating that the state of balance in the mean flow does not seem to matter, at least in homogenous turbulence.

We will make use of the total energy equation (Charney 1971)

$$\frac{\partial}{\partial t}\iint \frac{1}{2}\left[\frac{\delta(\nabla\psi_1)^2}{1+\delta} + \frac{(\nabla\psi_2)^2}{1+\delta} + \frac{\delta(\psi_1 - \psi_2)^2}{(1+\delta)^2 L_d^2}\right] dx\,dy + \frac{\delta(\overline{u_1} - \overline{u_2})}{1+\delta}\iint q_1 \frac{\partial}{\partial x}\psi_1\,dx\,dy + \frac{\delta(\overline{v_1} - \overline{v_2})}{1+\delta}\iint q_1 \frac{\partial}{\partial y}\psi_1\,dx\,dy$$
$$= -\frac{R_2}{1+\delta}\iint (\nabla\psi_2)^2\,dx\,dy + \text{ssd} \tag{7}$$

and the upper-layer potential enstrophy equation

$$\frac{\partial}{\partial t}\iint \frac{1}{2}\frac{\delta q_1^2}{1+\delta}\,dx\,dy + \frac{\delta}{1+\delta}\left[\beta + \frac{\overline{u_1} - \overline{u_2}}{(1+\delta)L_d^2}\right]\iint q_1 \frac{\partial}{\partial x}\psi_1\,dx\,dy + \frac{\delta(\overline{v_1} - \overline{v_2})}{(1+\delta)^2 L_d^2}\iint q_1 \frac{\partial}{\partial y}\psi_1\,dx\,dy = \text{ssd}. \tag{8}$$

Except where noted, the model domain size is $20\pi L_d$. We take $k^{-1} = \lambda/2\pi$, where k is wavenumber and λ is wavelength, as a measure of eddy length scale. Therefore a domain-filling eddy has a wavelength of $20\pi L_d$ and a length scale of $10L_d$. Our domain is smaller by a factor of 5 than that used in Larichev and Held (1995), who left more room for the inverse cascade to proceed away from L_d. We resolve activity near L_d, where most of the eddy energy resides (Stammer 1997), much better with our smaller domain. We set L_d to 50 km, a typical midlatitude value (Stammer 1997). Our dimensional domain size is then 3142 km; one much larger no longer plausibly represents a patch of a gyre.

We set $\sqrt{(\overline{u_1} - \overline{u_2})^2 + (\overline{v_1} - \overline{v_2})^2} = 1$ cm s^{-1} in our runs. Altimetric, current-meter, and hydrographic data (Wunsch 2001; Müller and Siedler 1992; Stammer 1997, respectively) indicate that 1 cm s^{-1} is a representative mean flow value in the midocean. Except where noted, we set $R_2 = (193 \text{ days})^{-1}$. The ''throughput''[1] parameter $\sqrt{(\overline{u_1} - \overline{u_2})^2 + (\overline{v_1} - \overline{v_2})^2}/R_2 L_d$, which measures the relative strengths of mean flow forcing and bottom Ekman friction, is 3.33. Weatherly and Martin (1978) estimate an abyssal bottom boundary layer depth d_{Ek} of about 10 m. Inserting this into the formula $R_2 = f_0 d_{\text{Ek}}/2H_2$ (cf. Pedlosky 1987) along with $H_2 = 4000$ m and $f_0 = 10^{-4}$ s^{-1} yields a decay rate of (100 days)$^{-1}$, indicating that our nominal decay rate may be reasonable. All plots in this paper are of nondimensional quantities. Energies are normalized by $[(\overline{u_1} - \overline{u_2})^2 + (\overline{v_1} - \overline{v_2})^2]/2$, PV and growth rates by $\sqrt{(\overline{u_1} - \overline{u_2})^2 + (\overline{v_1} - \overline{v_2})^2}/L_d$, time by $L_d/\sqrt{(\overline{u_1} - \overline{u_2})^2 + (\overline{v_1} - \overline{v_2})^2}$, and streamfunctions by $\sqrt{(\overline{u_1} - \overline{u_2})^2 + (\overline{v_1} - \overline{v_2})^2}L_d$.

The two-layer equations are integrated in the pseudospectral ''qgb'' model (Flierl 1994). A simple truncation at the Nyquist wavenumbers was employed to eliminate the worst effects of aliasing (LaCasce 1996). The time stepping scheme is third-order Adams–Bashforth. Except where noted, the experiments were initialized with fields randomly generated in physical space. Plots of total eddy energy versus time were inspected for each experiment. When no trend exists over a time at least as long as the spinup time (or, usually,

[1] We thank J. McWilliams for suggesting this name. It evokes an image of eddies growing from the mean flow and then being dissipated by bottom friction. In the weakly damped (high throughput) limit eddies turn over many times before feeling bottom friction.

longer), equilibration was judged to have been achieved. Except where noted, all of the results represent domain- and time-averages of equilibrated simulations with 256 squared resolution, using an exponential cutoff wavenumber filter for ssd.

LaCasce (1996) performed experiments with the same numerical model, initialized with a barotropic modon. Under hyperviscosity, the dipole loses energy fairly quickly and undergoes a distortion in shape. Under the wavenumber filter, energy decays slowly and distortions are minimal, more in line with inviscid analytical solutions. Our preference therefore is to use the wavenumber filter for ssd. In much of the parameter space explored in Arbic (2000), results do not strongly depend on whether a wavenumber filter or hyperviscosity is used for ssd. The vortex regime described in the current paper is sensitive to ssd and in vortex simulations we generally use hyperviscosity, at 128 squared resolution. Our numerical implementations of both types of ssd are described in the appendix.

3. Dependence of eddy energy on direction of mean shear flow

We define

$$P_S = \beta/\text{upper-layer shear gradient} = \beta(1 + \delta)L_d^2/\sqrt{(\overline{u_1} - \overline{u_2})^2 + (\overline{v_1} - \overline{v_2})^2}.$$

In this section $\beta = 2 \times 10^{-11}$ m^{-1} s^{-1}, a typical midlatitude value, which implies that $P_S = 6$. Our initial hypothesis therefore is that β dominates midocean mean PV gradients, and zonal flows are subcritical. Figure 2 plots maximum linear growth rates and equilibrated eddy energies versus angle of mean shear flow. Our convention is that 180°(270°/360°) represents westward (southward/eastward) shear. There is an asymmetry between the westward and eastward cases—see Riviere and Klein (1997) and references therein for a discussion. Due to frictional destabilization (Holopainen 1961) linear growth rates for purely zonal flows are nonzero. Both linear growth rates and equilibrated energies in the nonlinear problem are strong functions of angle. In the 270° experiment eddy energies are much higher than in observations. Researcher R. L. Panetta has performed similar calculations—see Panetta (1997) for preliminary results. Energies in the 190° and 185° experiments depend on initial condition. They are greater when spun up from the 195° experiment rather than from a random field. This is reminiscent of the hysteresis documented by Lee and Held (1991) in experiments with zonal mean flows. Zonal motions dominate in the experiments of this section because they are able to tap into available potential energy arising from meridional shears without crossing lines of constant PV. Snapshots of zonally averaged ψ_1 in four of the southeastward shear experiments are shown in Fig. 3. The large jump in energy seen in Fig. 2b between the 350° and 345° experiments is accompanied by a change from a wave to a jet regime.

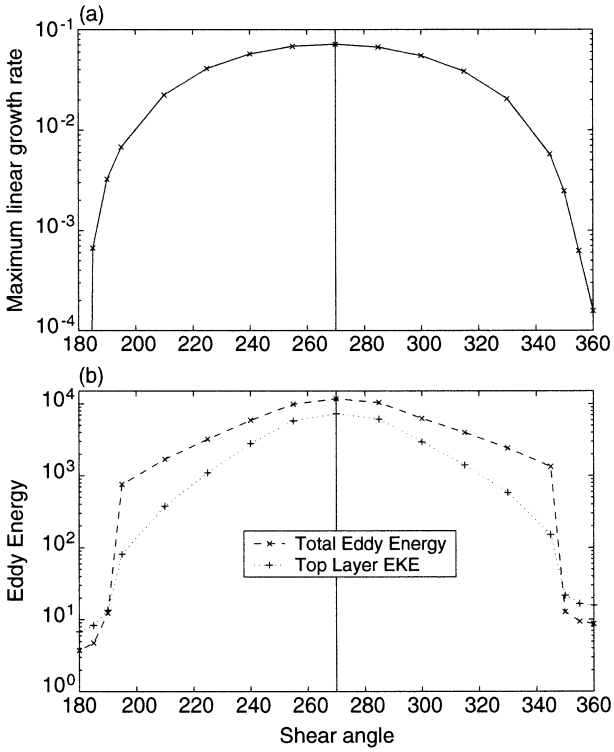

FIG. 2. (a) Maximum linear growth rate for $P_S = 6$, throughput = 3.33 experiments with parameters otherwise fixed, but with varying angle of shear flow. (b) Eddy energy in the equilibrated fully nonlinear simulations. Note that top-layer eddy kinetic energy is averaged over the upper layer only, while total eddy energy is averaged over the entire model depth. With these definitions top-layer eddy kinetic energy exceeds total eddy energy in some of the experiments.

4. Dependence of eddy isotropy on angle between layer mean PV gradients

In the preceding section, β dominates mean PV gradients. Eddies are anisotropic, consistent with earlier work linking β and anisotropy (Rhines 1975; Vallis and Maltrud 1993). Maps of midocean PV (Keffer 1985; O'Dwyer and Williams 1997) indicate that mean PV gradients often turn by order 90° in the thermocline. This implies that planetary and shear-induced mean PV gradients are of the same order, which contradicts our earlier inclinations. The discrepancy may be due to the fact that there is considerable shear within the thermocline. A two-layer model underestimates shear-induced gradients, even if given realistic mean flow values. For simplicity, we retain the two-layer model and our prescribed mean flow values, and examine the effect of varying β on eddy isotropy. In one set of experiments the shear flow angle is 330° (30° south of east), while in another set it is 210° (30° south of west). When β greatly exceeds shear-induced gradients, the angle between layer mean PV gradients is nearly zero. The angle

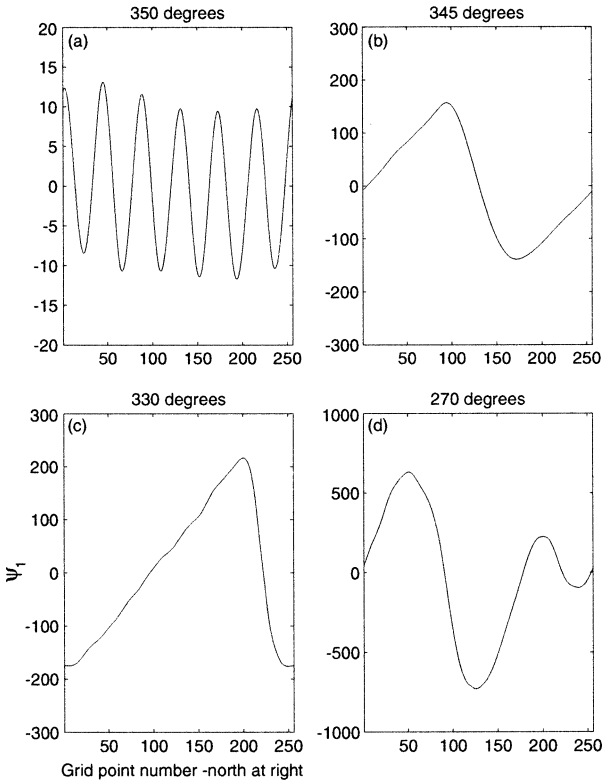

FIG. 3. Zonally averaged snapshots of ψ_1 from selected experiments in Fig. 2b.

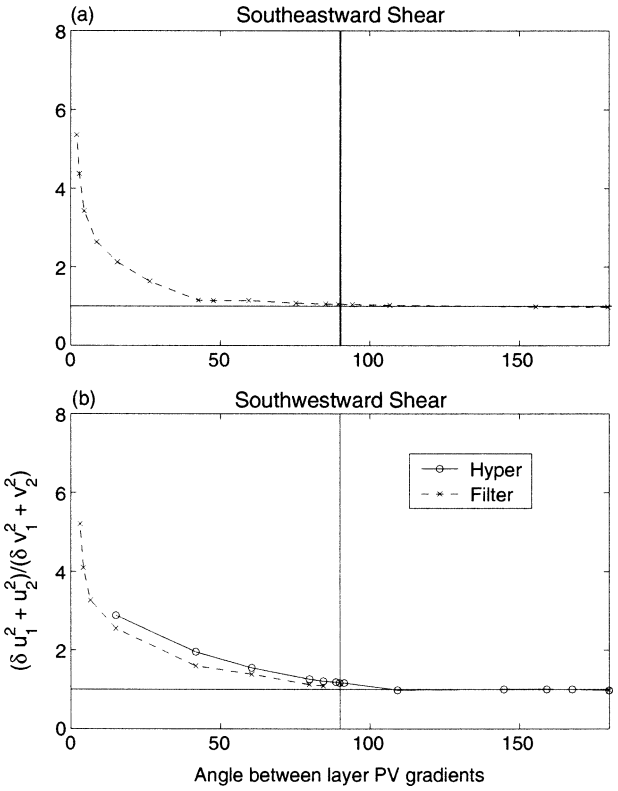

FIG. 4. Ratio of depth-averaged zonal to meridional kinetic energies vs angle between layer mean PV gradients, for (a) 330° and (b) 210° throughput = 3.33 experiments with varying beta. Extra vertical lines are drawn in at 90°. Extra horizontal lines are drawn in at the value of 1, which would indicate total isotropy. The hyperviscous experiments are run at 128 squared resolution.

exceeds 90° when P_S is order one or less. Figure 4 plots the ratio of layer-averaged zonal to meridional kinetic energies versus this angle. In both southeastward and southwestward simulations, when the angle is small, zonal motions dominate. In experiments with southeastward shear, complete isotropy (a ratio of zonal to meridional kinetic energies equal to 1) occurs when the angle between gradients exceeds 90°, although the ratio is close to 1 once the angle is about 50°. Evidently when the angle between layer mean PV gradients is large enough, no direction is imposed on the system and isotropy results. Current-meter data (cf. Table 1 of Wunsch 1997) suggest that in most locations zonal and meridional eddy kinetic energies are nearly equal, though there are large regional variations. In the southwestward experiments, when the angle between layer mean PV gradients exceeds approximately 90° and a wavenumber filter is used, fields of persistent isotropic vortices form. In this regime we have not achieved equilibration with a filter at resolutions higher than 64 squared. Equilibrated vortex states were obtained at higher resolutions with hyperviscosity. The hyperviscous vortex arrays are still highly energetic and model time steps must be small. Thus even 128 squared hyperviscous experiments are computationally expensive (about 10 processor days). Except where noted, the hyperviscous vortex experiments are at 128 squared resolution. They are used to complete Fig. 4b.

Figure 5 plots energy versus angle between gradients. For small angles (large β values) energy increases with increasing β and is larger than energy in f-plane flow (the latter is represented by the rightmost points in Figs. 4 and 5). This is contrary to expectations from linear stability analysis since β reduces growth rates. Neither f-plane nor large β experiments have a strong dependence on ssd. This provides confidence that our filter and hyperviscosity parameters are reasonable.

Snapshots of ψ_1 in the southeastward experiments are displayed in Fig. 6. The anisotropic large β solutions (Figs. 6a,b) are dominated by coherent jets that display a slow meridional drift. Figure 6c appears slightly anisotropic on the large scale but contains small isotropic features. As the angle between gradients increases (Fig. 6d), eddies take on an isotropic appearance similar to that of f-plane experiments (Fig. 8d). Snapshots of ψ_1 are shown for the southwestward experiments in Fig. 7 (which displays large β wavenumber filter experiments) and Fig. 8 (which displays small β hyperviscous experiments). Once again, jets dominate large β experiments, and experiments having an angle between gradients of approximately 40° (Fig. 7c) contain a mixture of isotropic and anisotropic features. Vortex arrays de-

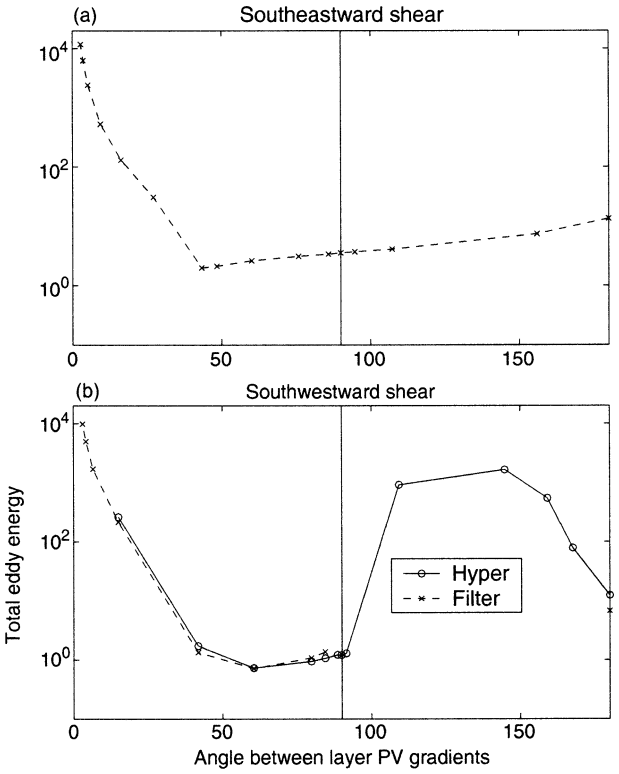

FIG. 5. Eddy energy vs angle between layer mean PV gradients for the simulations of Fig. 4.

velop with hyperviscosity when the angle between gradients is well beyond 90° (Figs. 8a–c). Vortex arrays were used to initialize the f-plane experiment shown in Fig. 8d but have disappeared by the time equilibration is reached. A nonzero β seems to be necessary for vortex arrays to arise and persist. Note that the vortex arrays described here are like-signed. As far as we know, these are the first QG simulations that show such a sign preference, other than cases in which the preference is imposed through initial or other conditions.

5. Coherent jets and vortices on the beta plane

Figure 9a plots total q_1 versus total ψ_1 for a snapshot of the 210°, $P_S = 3$, throughput = 3.33 jet solution (here total denotes the sum of eddy and mean contributions). Clear linear structure is present in between regions of near homogenization (Rhines and Young 1982). We therefore look for solutions to $q_1 = -\lambda\psi_1$, where λ is a constant. We suppose that variables are functions of y only, although the meanders present in the jet solutions imply that this is not strictly true. One solution is $\psi_1 = \text{const} \times y$ together with $\psi_2 = 0$. The first implies that $\nabla^2\psi_1 = 0$, and the second is consistent with the fact that friction is in the bottom layer. Figures 9b–d are qualitatively consistent with this solution. Zonally averaged ψ_1 rises nearly linearly over much of the

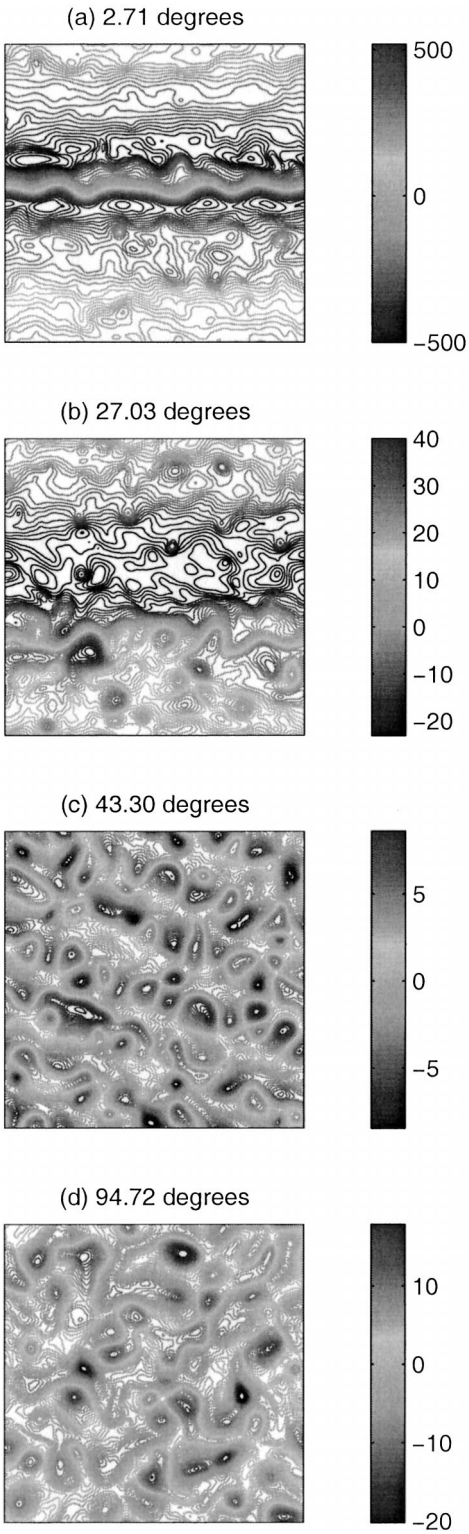

FIG. 6. Snapshots of ψ_1 for different angles between layer mean PV gradients in throughput = 3.33 experiments with direction of shear held fixed at 330° and varying beta.

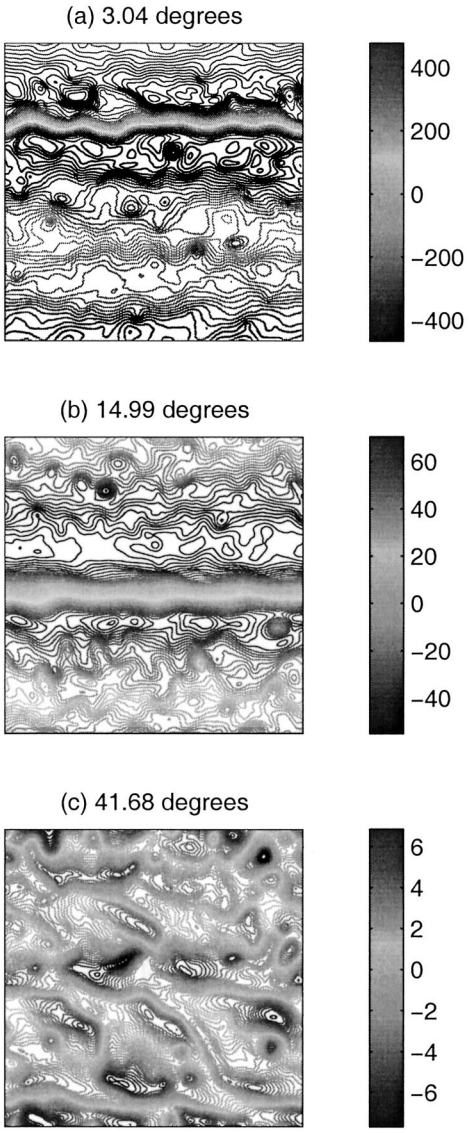

FIG. 7. As in Fig. 6 but with direction of shear held fixed at 210° and varying beta.

domain, and ψ_2 and $\nabla^2\psi_1$ are nearly zero so that q_1 is also linear. Total upper-layer PV is homogenized. Thus, as β increases, so must eddy amplitudes, consistent with the previously noted increase in eddy energy with β in the jet regime. In order to cancel β, ψ_1 rises from south to north over most of the domain in all jet solutions we have found. Double periodicity implies that ψ_1 cannot rise linearly throughout the entire domain. In the jet region it falls rapidly from south to north. Jet amplitude and structure change with throughput (not shown). For large throughput the jets widen, consistent with the familiar inverse cascade to larger scales (Batchelor 1953; Fjortoft 1953). For all throughput values, $\nabla^2\psi_1$ is nearly zero, however, ψ_2 is sizable for large throughput. Small throughput solutions are wavelike rather than jetlike.

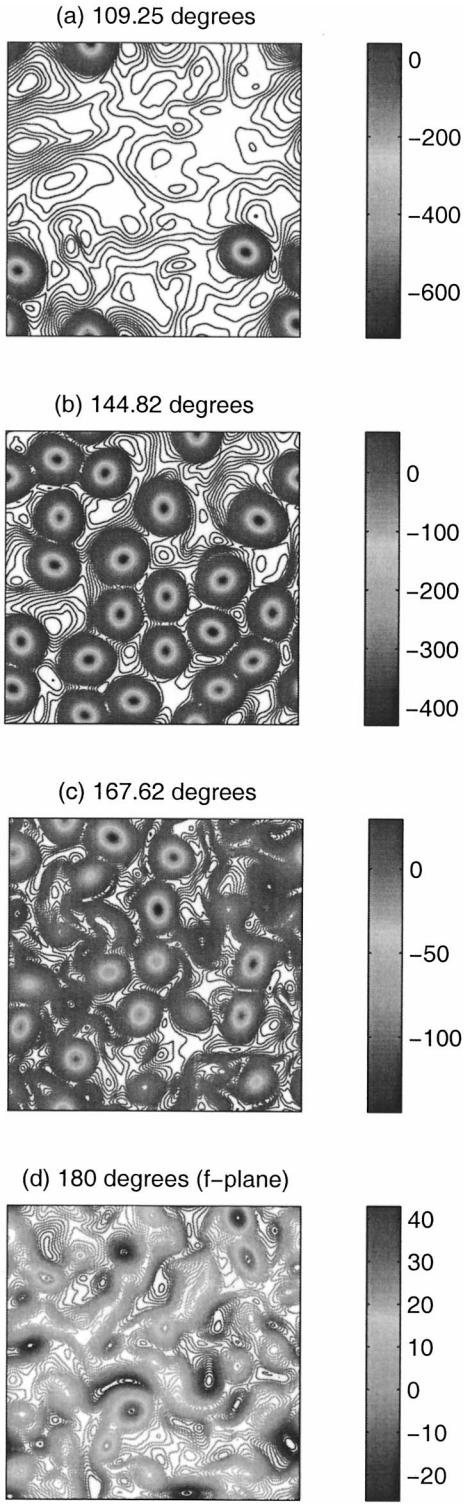

FIG. 8. As in Fig. 7 but small-scale dissipation is accomplished by hyperviscosity and resolution is 128 squared.

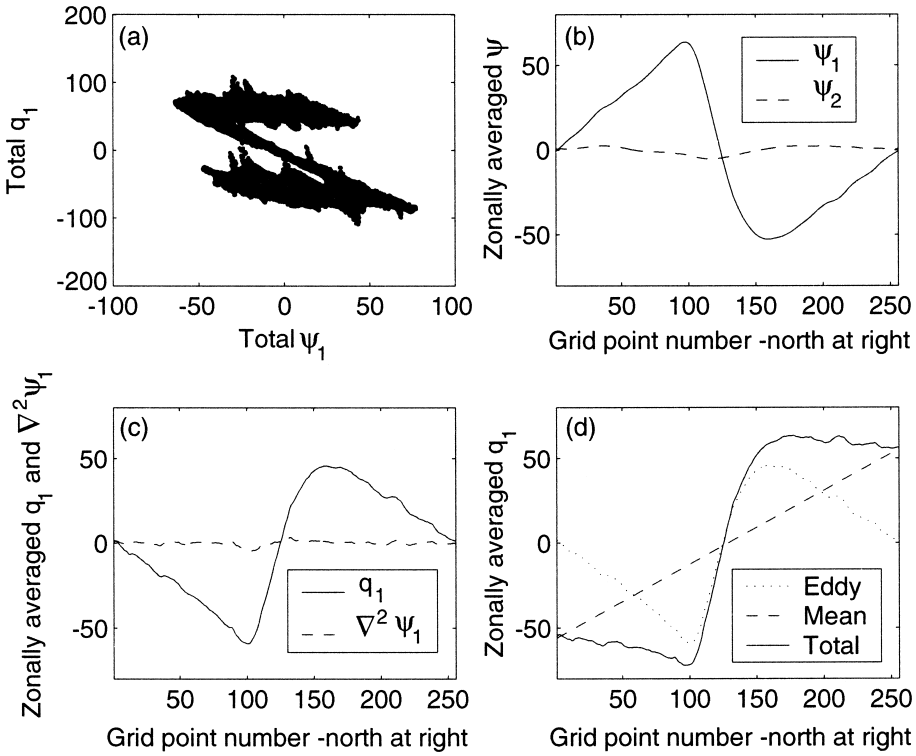

FIG. 9. Results from a snapshot of the 210°, $P_S = 3$, throughput = 3.33 experiment.

Thus the simple solution above holds only for a narrow range of order one throughput.

Rms evaluation of the terms in (1) reveals that the dominant balance in the upper layer of the vortex arrays is

$$\frac{\partial q_1}{\partial t} + J(\psi_1, q_1) \approx 0. \tag{9}$$

Individual terms in $J(\psi_1, q_1)$—that is, $u_1\partial q_1/\partial x$ and $v_1\partial q_1/\partial y$—are much larger than the Jacobian itself. This implies that q_1 is a strong function of ψ_1. Figures 10a and 10b plot q_1 versus ψ_1 for one equilibrated hyperviscous and one unequilibrated wavenumber filter vortex solution (each with a shear angle of 195° and 128 squared resolution). The scatterplots are tight and linear over much of the domain. In contrast, the q/ψ plot of an f-plane simulation with equal throughput (Fig. 10c) is rather shapeless. The q_1/ψ_1 plot of a weakly damped f-plane experiment (Fig. 10d; also, Arbic and Flierl 2003) has structure, but it is not linear—instead it resembles the sinh-like scatterplots of freely decaying f-plane flow (Montgomery et al. 1992; Brands et al. 1997). For the vortex regime, we consider the equation $q_1 = -\lambda\psi_1 - \alpha_1$ in cylindrical coordinates. We include a nonzero α_1 since vortex q_1/ψ_1 plots do not go through the origin. Since bottom motions are quite weak in the vortex regime, we set $\psi_2 \sim 0$, with solution

$$\psi_1 = \begin{cases} \alpha_1(1 + \delta)L_d^2 + \alpha_2 J_0(\kappa r), & \kappa r < 3.83, \\ \alpha_1(1 + \delta)L_d^2 + \alpha_2 J_0(3.83), & \kappa r > 3.83, \end{cases}$$

with

$$\kappa = \sqrt{\lambda - \frac{1}{(1 + \delta)L_d^2}}, \tag{10}$$

where r is a radial coordinate and 3.83 is the second zero in the slope of the Bessel function J_0. We have fit this solution to the snapshots in Figs. 10a and 10b. (Snapshots of ψ_1, ψ_2, and q_1 in physical space are shown in Fig. 11.) For each local vortex, we estimated the center position and peak value by fitting a quadratic surface to nine grid points centered on the point with the local minimum ψ_1 value. The values of ψ_1 for the 21 × 21 nearby points, normalized by the minimum, are plotted versus r/L_d in Fig. 12 for all 17 vortices in the hyperviscous case. The superimposed curve represents (10) similarly normalized. Given a choice of κ, we fixed the remaining parameter, the ratio of α_2 to α_1, by matching the curve to the average of the data values in the range $(3.83/\kappa L_d) - 0.1 < r/L_d < (3.83/\kappa L_d) + 0.1$. We then chose the value of κ that gave the best visual fit; it turns out to be $\kappa = 1/L_d$. For this value, which corresponds to $\lambda = (2 + \delta)/(1 + \delta)L_d^2 = 1.83/L_d^2$, we can model the interior of the vortices well, although Fig. 12 also shows that they have longer tails

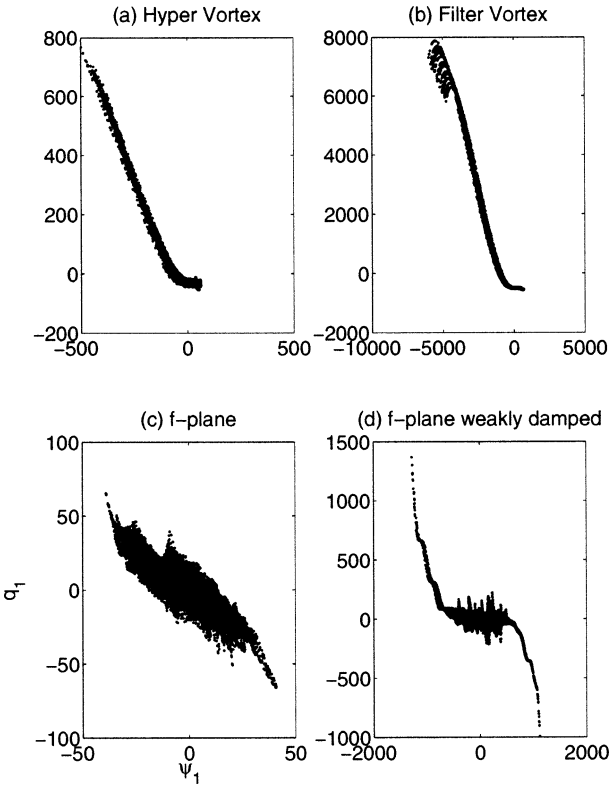

FIG. 10. Scatterplots of q_1 vs ψ_1 for snapshots of (a) 195°, P_S = 0.375, throughput = 3.33, 128 squared hyperviscous vortex solution; (b) 195°, P_S = 0.375, throughput = 3.33, 128 squared unequilibrated wavenumber filter vortex solution; (c) f-plane, throughput = 3.33 experiment; and (d) f-plane, throughput = 25 experiment.

than (10) predicts. The fit was not as successful for the filter solutions because of the nonlinear turning over at the top of the q_1/ψ_1 plot. Note that a least squares fit through the linear part of the hyperviscous q_1/ψ_1 scatterplot yields $\lambda = 1.90/L_d^2$, which is reasonably consistent with the above relation.

We can test the relative constancy of λ across different vortex solutions by plotting the ratio of total enstrophy to total energy against the variation of an important parameter, for instance, throughput. We relate this ratio to λ in the following argument, which also points toward a weak inverse cascade in the vortex regime. As before we take $\psi_2 \sim 0$, so $q_1 \approx \nabla^2\psi_1 - \psi_1/[(1 + \delta)L_d^2] \approx -\lambda\psi_1$. If we multiply by $-\psi_1$ and integrate, we obtain

$$\text{energy} \approx \lambda \iint \psi_1^2 \, dx \, dy. \tag{11}$$

If we square the approximate relation above and integrate, we get

$$\text{enstrophy} \approx \lambda^2 \iint \psi_1^2 \, dx \, dy. \tag{12}$$

(We have used the fact that the upper layer dominates total energy and enstrophy.) Thus domain-averaged total enstrophy over total energy will be approximately λ. This contrasts with purely two-dimensional turbulence, in which energy equals $\iint (\nabla\psi)^2 \, dx \, dy = \int E(k) \, dk$, and enstrophy equals $\iint (\nabla^2\psi)^2 \, dx \, dy = \int k^2 E(k) \, dk$, where $E(k)$ is the energy spectrum in wavenumber space. The factor of k^2 in the enstrophy integral leads to the inverse cascade (Batchelor 1953; Fjortoft 1953). Weakly damped f-plane turbulence behaves much like two-dimensional turbulence (Arbic and Flierl 2003). In the former case, as friction weakens, the inverse cascade strengthens, and we expect the enstrophy to energy ratio to change accordingly. In the beta-plane vortex regime, the approximate enstrophy integral (12) lacks the factor of k^2, and we expect the inverse cascade to be diminished in strength. Figure 13 plots enstrophy over energy versus throughput for 128 squared, 195°, P_S = 0.375 hyperviscous vortex experiments and 256 squared wavenumber filter f-plane simulations. The ratio is indeed more nearly constant in the beta-plane vortex regime. Changing β, shear angle, and initial conditions within the vortex regime also does not dramatically change the enstrophy over energy ratio. It lies between $1.2/L_d^2$ and $1.5/L_d^2$ in all of the experiments examined. The implied value of λ is lower than in the Bessel-fitting exercise, which used only vortex cores, with their steep linear q_1/ψ_1 relationships.

Figure 14 plots various quantities versus throughput in the 128 squared, 195°, P_S = 0.375 hyperviscous vortex experiments. Again, f-plane solutions are plotted alongside. Energies of both sets increase with decreasing friction when throughput is order 1 and larger. The f-plane experiments undergo the familiar inverse cascade to large horizontal scales and the barotropic mode[2] (Charney 1971; Rhines 1977; Salmon 1978, 1980) as friction decreases in the weakly damped limit. Upper-layer kinetic energy of the vortex arrays greatly exceeds that of the lower layer, and upper-layer length scale[3] is near L_d, even when friction is weak. This is consistent with (10) and the argued weakness of the inverse cascade in the vortex solutions. As throughput drops below 1, visual inspection of snapshots indicates that the like-signed vortex arrays cease to exist. This is corroborated by the rapid decrease in skewness and the increase in its variability during integrations (Fig. 15). The skewness plot emphasizes the persistent, like-signed nature of the beta-plane vortices, in contrast to f-plane turbulence, in which skewness changes sign during simulations.

As throughput increases, the vortex lattices become more spread out in physical space (not shown). We do not know if there is a nonzero value of R_2 below which vortex arrays cease to form. When bottom friction is zero, the cascade to barotropic domain-scale flow takes

[2] The barotropic and baroclinic streamfunctions are respectively defined by $\psi_{BT} = (\delta\psi_1 + \psi_2)/(1 + \delta)$, $\psi_{BC} = \sqrt{\delta}(\psi_1 - \psi_2)/(1 + \delta)$.

[3] This is estimated as the reciprocal of the first moment (centroid) of the upper-layer kinetic energy wavenumber spectrum.

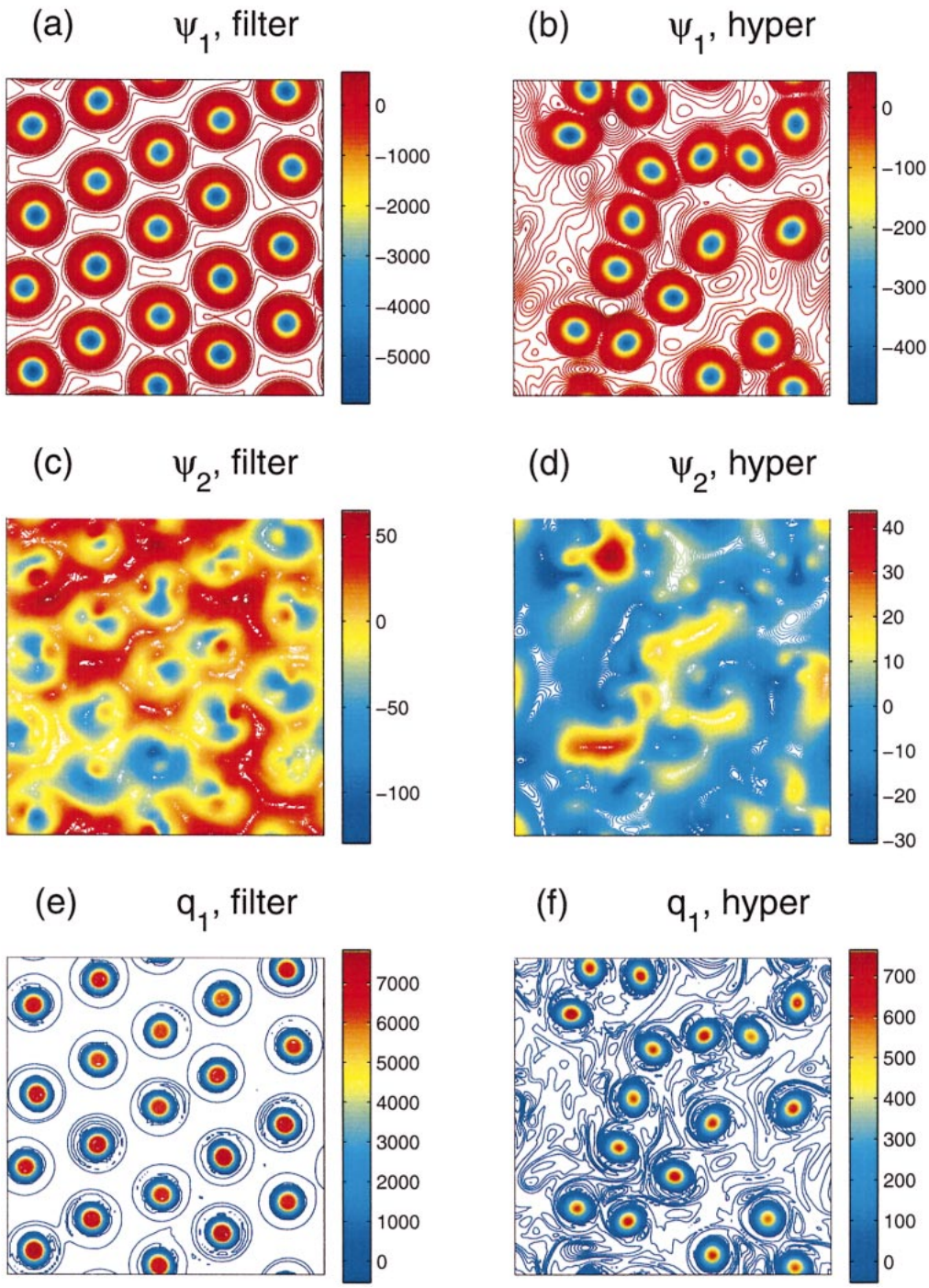

FIG. 11. Snapshots of ψ_1, ψ_2, and q_1 for 128 squared, 195°, $P_S = 0.375$, throughput = 3.33 experiments with wavenumber filter and hyperviscosity. The filter experiment is unequilibrated.

place in the form of one large monopole. Thus skewness persists but the solution is not at L_d scales. Vortex lattices also do not form (or persist, when put in as an initial condition) when there is symmetric Ekman friction (i.e., when an upper-layer friction R_1 is put in that is equal to R_2). This is consistent with the absence of vortices in the ψ_2 field (Fig. 11). The beta-plane vortices require friction to be present and in the bottom layer only.

The vortex arrays are sensitive to ssd. Starting from small-scale random initial conditions, 64 squared, 128 squared, 256 squared, and 64 squared double resolution

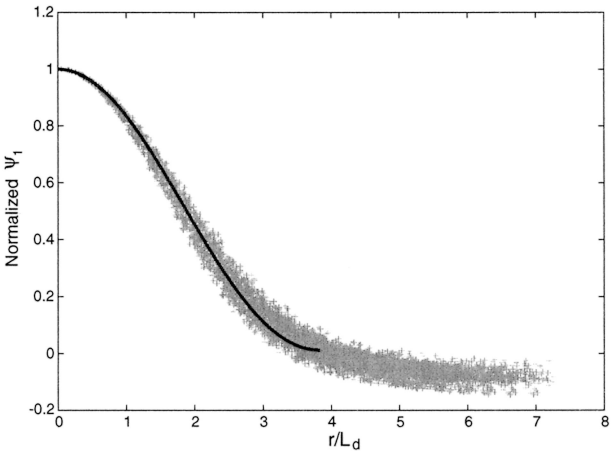

FIG. 12. Bessel function fit (solid line) to ψ_1 values around the vortex cores in Fig. 11b.

(half domain size) simulations were performed with a wavenumber filter, a shear angle of 195°, and $P_S = 0.375$. Vortex lattices emerged at all of these resolutions, but at high resolution we were unable to attain equilibration (Fig. 16) despite integrating for several months. Energies continue to rise, forcing us to adopt ever smaller time steps until the simulation becomes unfeasible and energies greatly exceed oceanographically plausible values. We have achieved equilibration in the vortex regime with hyperviscosity (ssd = $\nu\nabla^{2n}q$). The range of ν values over which vortex solutions emerge widens as the order of hyperviscosity increases. We did not find vortex arrays at 128 squared resolution when n was less than 3. In the hyperviscous experiments shown in this

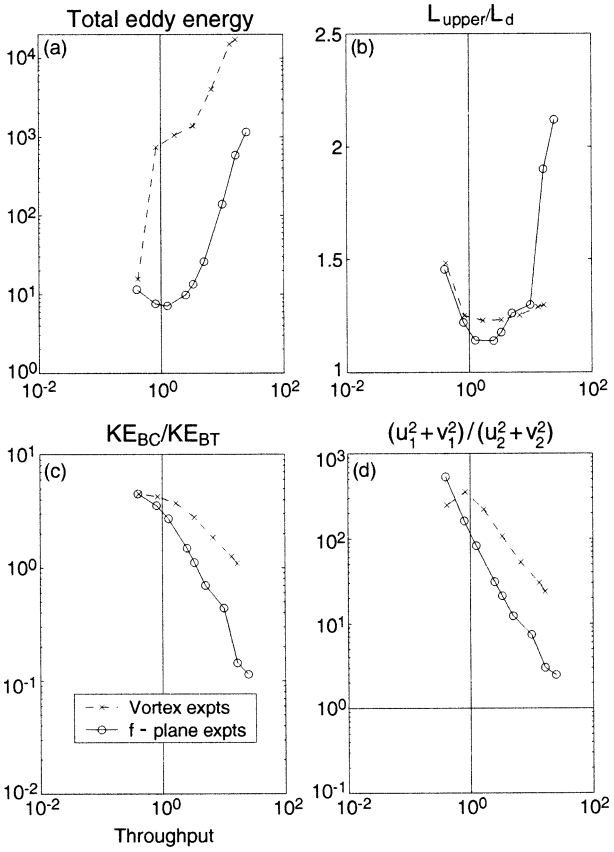

FIG. 14. Comparison of 195°, 128 squared, $P_S = 0.375$ hyperviscous vortex solutions to f-plane solutions as a function of throughput.

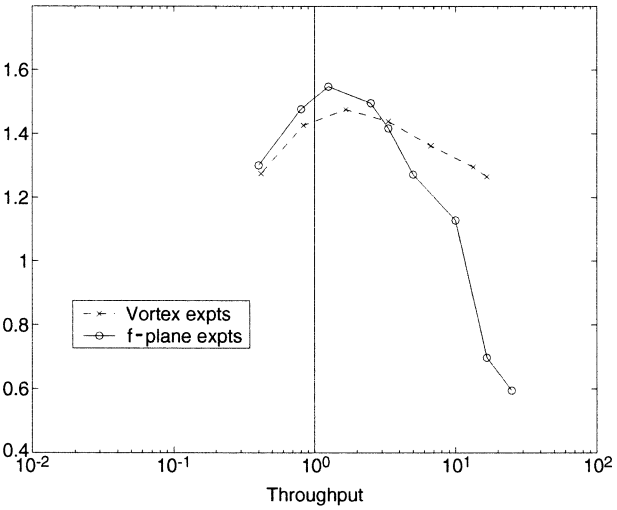

FIG. 13. Plot of L_d^2(total energy)/total enstrophy vs throughput for 195°, 128 squared, $P_S = 0.375$ hyperviscous vortex solutions and f-plane solutions. Total energy is

$$\frac{1}{2}\left[\frac{\delta(\nabla\psi_1)^2}{1+\delta} + \frac{(\nabla\psi_2)^2}{1+\delta} + \frac{\delta(\psi_1-\psi_2)^2}{(1+\delta)^2 L_d^2}\right],$$

and total enstrophy is $(\delta q_1^2 + q_2^2)/2(1+\delta)$.

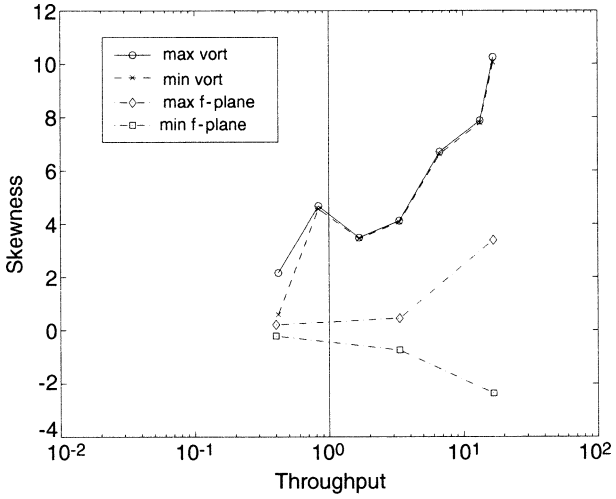

FIG. 15. Maximum and minimum skewness of q_1, plotted vs throughput for 195°, $P_S = 0.375$, 128 squared hyperviscous vortex experiments (all cyclonic) and selected f-plane experiments. Skewness is defined as $\langle q_1^3\rangle/\langle q_1^2\rangle^{3/2}$, where angle brackets denote a domain average, and is calculated for several snapshots for each simulation. The snapshots are well spread out in time and are taken after equilibration is reached.

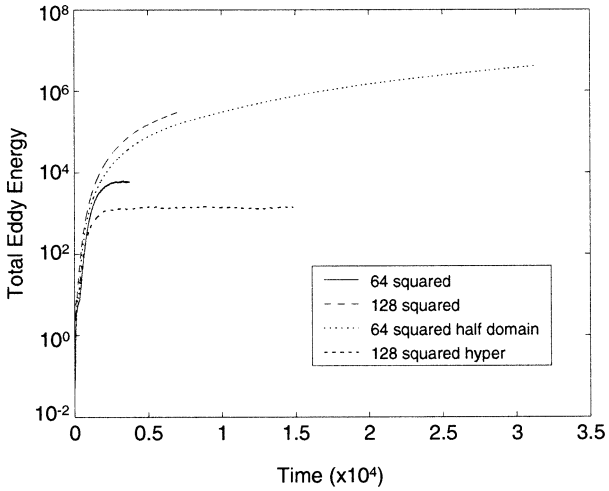

FIG. 16. Energy vs time for 195°, $P_S = 0.375$, throughput = 3.33 experiments. Wavenumber filter solutions were run at 64 squared, 128 squared, and 256 squared (not shown) resolution, as well as 64 squared resolution at one-half of the domain size. Resolution of the hyperviscous solution is 128 squared. Equilibration has occurred only in the 64 squared wavenumber filter and 128 squared hyperviscous experiments.

paper, we use ssd $= \nu\nabla^6 q$. Our chosen ν value damps the L_d length scale (wavelength $2\pi L_d$) at a rate 300 times less than the Ekman friction value (193 days)$^{-1}$ damps all scales. As seen in Fig. 11, the hyperviscous vortices are less circular and less regularly spaced than the wavenumber filter vortices.

We believe that sensitivity to ssd, while somewhat unsettling, is a consequence of the weak inverse cascade in the vortex regime. Since upper-layer enstrophy is continually being produced from the mean flow, a steady state can only be obtained if there is some enstrophy dissipation in the upper layer, which must be accomplished by ssd [Eq. (8)]. Since the inverse cascade is suppressed, enstrophy transfer to small scales is diminished, and substantial enstrophy dissipation can take place only if ssd acts at scales that contain most of the enstrophy. Integrals (11) and (12) imply that most of the enstrophy will be at the same scales that contain most of the energy—that is, L_d scales. As we increase resolution in our wavenumber filter solutions, the cutoff scale (see the appendix) moves to scales much smaller than L_d and vortex amplitudes increase dramatically as a result. Hyperviscosity affects all scales, including those near L_d, and thus makes equilibration easier. We interpolated the hyperviscous solution in Fig. 11b onto 256 squared resolution and continued it with the same ν value; no difference in energy or other eddy characteristics resulted. We choose not to perform experiments with higher resolution and lower ν because we expect such experiments, like the filter simulations with a reduced cutoff scale, to have extremely large energies. Given our argument that upper-layer enstrophy dissipation occurs near L_d scales and that significant energy resides at those scales, we might expect substantial upper-layer energy dissipation in the vortex arrays. In the hyperviscous vortex solutions as well as the 64 squared equilibrated wavenumber filter vortex solutions, upper-layer small-scale dissipation accounts for about 10%–17% of the total energy dissipation. This contrasts with our f-plane simulations, in which bottom Ekman friction accounts for all but two percent of the energy dissipation. On the f plane, the inverse cascade is stronger, so enstrophy dissipation need not occur at scales large enough to affect the energy.

Experiments initialized by vortex fields, but in which the mean flow is omitted while Ekman friction is retained, show energy decay over time scales much less than the length of the forced–dissipated experiments. This demonstrates that energy extraction from the mean flow is essential for vortex array maintenance. The extraction is slow, consistent with the weakness of lower-layer motions, and thus of dissipation. The ratio of nondimensional energy to nondimensional energy production is 870 for the hyperviscous vortex solution of Fig. 11, and is only 100 in f-plane simulations with equal throughput.

Vortex fields can form in mean flows that are very slightly east of south (or north), in meridional flows, and in flows with a westward zonal component, as long as β is nonzero but small enough so that the angle between layer mean PV gradients exceeds approximately 90°. Transition to vortex solutions takes place at supercriticality in the purely westward case. In the hyperviscous vortex regime, where equilibration has been obtained, energy dependence on shear angle is much less than in the large β jet regime. We use (2), with hyperviscosity as ssd, to illustrate symmetry properties:

$$\frac{\partial q_2}{\partial t} + \overline{u_2}\frac{\partial q_2}{\partial x} + \overline{v_2}\frac{\partial q_2}{\partial y} - \frac{\delta(\overline{v_1} - \overline{v_2})}{(1+\delta)L_d^2}\frac{\partial \psi_2}{\partial y} + \left[\beta + \frac{\delta(\overline{u_2} - \overline{u_1})}{(1+\delta)L_d^2}\right]\frac{\partial \psi_2}{\partial x} + J(\psi_2, q_2) = -R_2\nabla^2\psi_2 + \nu\nabla^6 q_2. \quad (13)$$

If $\overline{u_1}$ and $\overline{u_2}$ both change sign, the shear part of $\partial\overline{q_2}/\partial y$ reverses sign. However, β does not. Therefore (13) is not invariant to a change in sign of the zonal mean velocities. If Ekman friction were vertically symmetric, then, in the $\delta = 1$ case at least (in which vortex arrays also develop), upper- and lower-layer subscripts could be switched and the layer PV equations would be invariant. However, when Ekman friction acts only in the

bottom layer, the indices cannot be switched. Thus the asymmetry in vortex formation between eastward and westward mean flows is connected to the vertical asymmetry of Ekman friction.[4]

All vortex fields presented thus far are cyclonic. Let us consider whether an equilibrated cyclonic solution multiplied by -1 is also a solution. Reversing the sign of ψ_2 and ψ_1 changes the sign of all the terms in (13) save the Jacobian. The Jacobian changes sign if one (but not both) of the spatial coordinates changes sign. Since β and the mean shear both impose a direction, the presence of either limits the choice of spatial coordinates to invert. For instance, if $\overline{v_1}$ and $\overline{v_2}$ were zero but β were nonzero, then (13) would be invariant under $\psi_1 \rightarrow -\psi_1$, $\psi_2 \rightarrow -\psi_2$, $y \rightarrow -y$ (cf. McWilliams and Flierl 1979), but not under $\psi_1 \rightarrow -\psi_1$, $\psi_2 \rightarrow -\psi_2$, $x \rightarrow -x$. The most general case of (13)—a nonzonal flow on a beta plane—is not invariant under either of the above transformations since layer mean PV gradients are not colinear. Equation (13) is invariant under the transformations $\psi_1 \rightarrow -\psi_1$, $\psi_2 \rightarrow -\psi_2$, $y \rightarrow -y$, $\overline{v_1} \rightarrow -\overline{v_1}$, and $\overline{v_2} \rightarrow -\overline{v_2}$. This was tested by flipping an equilibrated hyperviscous vortex solution $\psi(x, y)$ to $-\psi(x, -y)$ in both layers, flipping the mean meridional flow, and continuing the experiment. The number of anticyclones stayed constant, as did the time-averaged energy. Experiments confirmed that a vortex array formed in a westward purely zonal flow is invariant under $\psi \rightarrow -\psi$, $y \rightarrow -y$. On the other hand, if β and $\overline{v_1} - \overline{v_2}$ are nonzero and held fixed, symmetry breaking occurs. We performed one experiment with the same parameters as in Fig. 11b, but with the initial condition taken to be the snapshot in Fig. 11b multiplied by -1. The vortices remain anticyclonic, but energy decreases by an order of magnitude. Thus, if the mean shear is southwestward (northwestward), energy levels are higher (lower) for a field of cyclones than for a field of anticyclones. A variety of initial conditions were tested with parameters as in the hyperviscous experiment in Fig. 11b. Vortex solutions always formed. Initial conditions that were random in wavenumber space or physical space yielded high-energy cyclones. Equilibrated solutions from other parts of parameter space explored in Arbic (2000), for instance, strongly and weakly damped f-plane solutions, and a beta-plane jet solution, were also used as initial conditions. The latter two led to low-energy anticyclones. Thus for southwestward mean flows most initial conditions seem to produce high-energy cyclones.

We conclude this section by noting that our model conserves the domain integral of q and that this is zero to within numerical accuracy in all our simulations. In the vortex experiments, small vortex core regions with large q values are balanced by larger regions having q values of smaller magnitude and opposite sign. We also note that the wavenumber spectra of vortex arrays formed with either hyperviscosity or a wavenumber filter are not red out to the largest scales. Thus the arrays are not affected by the size of the domain.[5]

6. Discussion

Previous work on homogeneous baroclinically unstable beta-plane geostrophic turbulence has been done with eastward zonal mean flows (cf. Panetta 1993; Held and Larichev 1996; Smith and Vallis 2002). Here we have allowed the mean flow to have an arbitrary direction, and uncovered a rich parameter space. When planetary beta dominates mean PV gradients, eddy energy greatly increases as the mean shear turns away from an east–west orientation. Additional experiments (not shown for the sake of brevity) indicate that energy also increases with shear angle when beta is weaker, although in some parts of parameter space the increase is large only when friction is weak. All of this suggests that even weak midocean gyre flows, because of their meridional component, may generate substantial eddy energy. Our contribution in this regard complements that of many linear stability analyses as well as that of Dubus (1999) and Spall (2000), which reached similar conclusions in fully nonlinear simulations driven by inhomogeneous mean flows. Interestingly, according to maps in Wunsch (2001), the Antarctic Circumpolar Current has one of the lowest ratios of eddy to mean kinetic energy in the World Ocean. Perhaps this is because the mean flow there is nearly zonal.[6] We have attempted without success to produce a scaling argument, in the spirit of those in Held and Larichev (1996) and Spall (2000), for eddy energy in our experiments. Spall's scaling predicts a decrease in eddy energy with increasing beta, opposite to the behavior in our large beta jet regime. The discrepancy is probably due to the periodic boundaries in our experiments, which permit jets that are not present in his study.

Midocean potential vorticity maps indicate that mean PV gradients undergo considerable turning in the thermocline, which suggests that planetary and shear-induced gradients are of comparable magnitude. We have demonstrated here that eddy isotropy in baroclinically unstable beta-plane turbulence depends on the angle between layer mean PV gradients, which depends on mean shear flow direction and the ratio P_S of planetary to shear-induced gradients. When the angle between layer gradients is small, zonal motions dominate. When the angle between gradients exceeds approximately 90°, no direction is imposed on the system, and zonal and meridional kinetic energies are nearly equal. Thus, the near-isotropy of midocean eddies may be related to the twisting of mean PV gradients.

[4] We thank M. Spall for raising this issue and I. Held for clarifying discussions.

[5] We thank A. Provenzale for raising this issue.

[6] We thank J. Marshall for pointing this out to us.

In contrast to the f plane, on the β plane coherent structures can form when throughput has order-1 values, which we have argued are appropriate for the midocean. When β dominates layer mean PV gradients and the mean shear has a significant meridional component, coherent zonal jets develop. The narrowness of our order-one throughput jet solutions (cf. Figs. 3c, 6a, and 7a) contrasts with the jets in Panetta (1993). His jets, which apparently arose only with weak friction, were not much narrower than the interjet spacing (see his Fig. 7). Panetta (1993) did not discuss the q/ψ relationships of his simulations. If β is nonzero but small enough to permit isotropy and the zonal component of the mean flow is not strongly eastward, lattices of coherent like-signed vortices develop in our simulations. Our coherent jets and vortices were not imposed in the initial conditions. They arise spontaneously as do the vortices in the freely decaying experiments of McWilliams (1984). As far as we know, Arbic and Flierl (2003) and the present paper are the first studies of tight q/ψ relationships in models having stratification, forcing, and dissipation present simultaneously. Like-signedness and differing energy levels for cyclonic and anticyclonic arrays distinguish the present vortices from those previously studied in two-dimensional, equivalent barotropic, and stratified QG turbulence. Freely decaying shallow-water and SQG + 1 turbulence exhibits cyclone/anticyclone asymmetry (Charney and Flierl 1981; Polvani et al. 1994; Hakim et al. 2002), but the nature of the asymmetries in our study is different. Here, asymmetry arises from the imposed mean state, and vortices are all like-signed within a particular solution. In freely decaying shallow-water turbulence cyclones and anticyclones coexist, but in different numbers. Our experiments suggest that there may be more coherent vortices in that part of the gyre having westward zonal mean shear. Furthermore, gyre regions having southwestward (northwestward) mean shear may show a preference for cyclones (anticyclones). However, it is not clear that these aspects of our simple model will extrapolate successfully to the actual ocean.

In the vortex regime the inverse cascade to large-scale barotropic motions is diminished in strength relative to that in other flat-bottom QG turbulence simulations. We have argued that this suppression of the inverse cascade is linked to the linear q/ψ scatterplots and is behind the sensitivity to ssd displayed by the vortex solutions. In contrast, weakly damped f-plane solutions (Fig. 10d; also, Arbic and Flierl 2003) have sinh-like q/ψ scatterplots, as in freely decaying two-dimensional flow (Montgomery et al. 1992), and a strong inverse cascade.

There is no creation or destruction of the beta-plane vortices after equilibration occurs, and only weak interaction amongst them. We have ascertained this from watching movies of long integrations, and from the stability of skewness during integrations. Vortex lattices persist despite the presence of bottom friction because they are able to draw energy from the mean flow. Assuming that similar processes occur in the actual ocean, midocean friction strengths would be underestimated if they are measured by the lifetime of individual eddies, which can exceed a year or so.

The fact that vortices form when the mean flow has a westward zonal component, but not an eastward one, is due to β (the f plane is rotationally invariant) and the vertical asymmetry of friction. Vortex fields form in the upper layer where there is no Ekman friction. Equations (7) and (8) imply that the ratio of upper-layer enstrophy to total energy production is reduced relative to that on the f plane for westward flows on a beta plane, but is increased in eastward flows. This suggests that a reduction in upper-layer enstrophy production, together with isotropic conditions, might play a role in coherent vortex formation. (Note, however, that vortex arrays also form in experiments with zonal mean flows and a small β present only in the bottom layer, which leaves upper-layer enstrophy production unaffected.) The ratio is similarly reduced in our large β jet solutions. This suggests that a reduction in upper-layer enstrophy production together with strong anisotropy might be involved in the formation of coherent jets. These enstrophy production conjectures, if correct, may be related to the minimum enstrophy arguments for unforced systems given by Stern (1975) and Bretherton and Haidvogel (1976), whose solutions also had linear q/ψ relationships.

Several aspects of the vortex solutions require further study and explanation, for instance: their sensitivity to ssd, their lattice nature, their like-signedness, and the different energy levels for states of cyclones and anticyclones. We have not been able to predict the slopes that form in the q/ψ relationships. A complete theory of the vortex arrays will probably have to consider their propagation speeds. We have roughly estimated the speed of the lattice shown in Fig. 11a by tracking individual vortices across the domain. Although oscillations occur, the mean position clearly propagates, in a direction 15° north of west. The lattice propagation speed appears to be 2.5 times as fast as the mean shear. The frame in which the lattice is nearly steady may be the appropriate one in which to seek a complete analytical solution.

The crystalline structure in the vortex arrays is somewhat similar to that seen by Kukharkin et al. (1995) and Smith et al. (2002) in simulations of forced–dissipated equivalent barotropic turbulence, but their crystals were less regular and no sign preference was noted. Vortex crystals have been formed in laboratory experiments of freely decaying two-dimensional turbulence (Fine et al. 1995; see Schecter et al. 1999 and Jin and Dubin 2000 for related theoretical and numerical work). In this case, however, crystal formation is very sensitive to initial condition and may require nonzero domain-averaged vorticity (D. Schecter 2003, personal communication). In the present forced–dissipated simulations, vortex arrays of one sign or another have formed with all initial

conditions we have tried, and all of our initial conditions have zero domain-averaged vorticity.

An important parameter in our work is the throughput $\sqrt{(\overline{u_1} - \overline{u_2})^2 + (\overline{v_1} - \overline{v_2})^2}/R_2 L_d$. An equivalent parameter in a multilayer model would depend on the deformation radii of higher baroclinic modes as well as the modal structure of the mean shear. Hua and Haidvogel (1986) and Smith and Vallis (2001, 2002) found in multilayer simulations that the higher baroclinic modes have less energy than that in the first baroclinic mode. This, along with the fact that the mean shear in the midocean projects primarily onto the first baroclinic mode, suggests that our two-layer model and throughput parameter probably capture most of the physics.

Our viewpoint in this paper has been that equilibrated turbulence driven by horizontally homogeneous mean flows and damped by bottom friction is a reasonable model for the generation of midocean eddies via baroclinic instability. In homogeneous models there are no eddy flux divergences, thus mean flows are unaffected by eddy feedbacks. In weakly nonlinear channel models of baroclinic instability (Pedlosky 1970), eddy flux divergence significantly alters mean flows, and therefore affects eddy equilibration. In this case friction is still involved in the equilibration process, but the mean flow is no longer homogeneous. If midocean mean flows were indeed significantly altered by eddy flux divergence, our homogeneous model would not be valid. We wish to judge whether eddy flux divergences significantly alter midocean mean flows before losing their energy through bottom friction. We do so by estimating the time scale for divergence to affect the mean flow and comparing it to typical frictional spindown time scales.[7] Eddy PV flux divergences alter zonal mean flows via $d\overline{q}/dt = -d\overline{vq}/dy$, where overbars denote a zonal average (Pedlosky 1987). Thus eddies will eliminate the meridional mean PV gradient $d\overline{q}/dy$ over the time scale

$$T_{\text{feedback}} \sim \frac{L_{\text{mean}}(d\overline{q}/dy)}{d\overline{q}/dt} \sim \frac{L_{\text{mean}}^2}{vL_{\text{eddy}}}, \tag{14}$$

where L_{mean} is the scale over which the mean flows vary, and we have scaled d/dy as $1/L_{\text{mean}}$ and q as $L_{\text{eddy}}d\overline{q}/dy$. If we take $L_{\text{mean}} \sim 1000$ km (a patch of the gyre, rather than the entire gyre), $v \sim 10$ cm s^{-1}, and $L_{\text{eddy}} \sim 100$ km we obtain $T_{\text{feedback}} \sim 1000$ days. A similar scaling could be applied to erase the zonal gradients $d\overline{q}/dx$. In that case the relevant PV flux would be $d\overline{uq}/dx$. Following Spall (2000), we assume that zonal motions tapping into zonal gradients occur on basin scales since they are not constrained by planetary beta. Then $q \sim L_{\text{mean}}d\overline{q}/dx$, leaving $T_{\text{feedback}} \sim L_{\text{mean}}/v \sim 100$ days, less by a factor of $L_{\text{mean}}/L_{\text{eddy}}$. If L_{mean} were taken to be a typical basin length, say, 4000 km, feedback times increase to 16 000 and 400 days. We conclude that zonal gradients can be erased in 100–400 days, while approximately 1000–16 000 days are required to erase the meridional gradients. If, as argued in section 2, frictional spindown times are indeed substantially less than 1000 days, then eddy flux divergence probably does not significantly alter midocean mean flows. Our model of eddy equilibration by friction in a homogeneous mean flow seems therefore to be a reasonable approximation for the midocean. The above argument is, however, rough and subject to revision.

Acknowledgments. BKA is profoundly grateful to numerous individuals, listed in the acknowledgments of Arbic (2000), for helping him in various ways to complete his Ph.D. thesis. As that work was further developed into this paper, BKA had helpful discussions with more people, including David Schecter, David Nolan, Melvin Stern, Steve Griffies, Lee Panetta, Ben Cash, Patrice Klein, Ted Shepherd, Peter Rhines, and Man-Kin Mak. Shafer Smith and Jim McWilliams were particularly helpful, as was Guillaume Lapeyre, who read the manuscript and suggested many improvements. Two anonymous reviewers also greatly improved the manuscript with their comments. Cathy Raphael prepared the final version of the figures. Many people at MIT, WHOI, and GFDL allowed BKA to use their computers. While this research was undertaken, BKA was funded by an Office of Naval Research/National Defense Science and Engineering Graduate Fellowship, Office of Naval Research Grant N00014-95-1-0824, and National Science Foundation Grant OCE-9617848. GRF was also supported by the National Science Foundation grant. This paper was written while BKA was supported by the GFDL/Princeton University Visiting Scientist Program.

This paper is dedicated to the memory of Constantine Giannitsis, a colleague of both authors, a close friend, and a graduate student classmate of BKA. He was a truly unique individual, whose enthusiasm for science and life is sorely missed.

APPENDIX

Implementations of Small-Scale Dissipation

The exponential cutoff wavenumber filter (cf. Canuto et al. 1988) we use is of the form

$$\text{filter} = \begin{cases} \exp[-\alpha(k - k_0)^M] & \text{when } k > k_0, \\ 1.0 & \text{when } k \le k_0, \end{cases} \tag{A1}$$

where k is the total wavenumber, and k_0 is a cutoff wavenumber. The 256 squared experiments used the same parameter values as LaCasce (1996): $\alpha = 18.4$, $M = 4$, and k_0 is 0.65 times the Nyquist wavenumber. The filter is applied to $\hat{q}$, the Fourier transform of q, at every time step.

When hyperviscosity is used, the equation that must be solved within each layer is

[7] We thank J. Pedlosky for suggesting that we seek such a scaling.

$$\frac{\partial}{\partial t}\widehat{q_N} = \mathrm{OT} - \nu k^{2n}\widehat{q_N}, \tag{A2}$$

where N is the layer index, and OT stands for other terms in the equation. Direct evaluation of (A2) is difficult since k^{2n} becomes large for large wavenumbers and small time steps are needed for numerical stability. To circumvent this, a ''semi-implicit'' scheme is widely used:

$$\widehat{q_N}(t + \Delta t) - \widehat{q_N}(t) = \Delta t\mathrm{OT} - \Delta t\nu k^{2n}\left[\frac{\widehat{q_N}(t + \Delta t) + \widehat{q_N}(t)}{2}\right], \tag{A3}$$

with solution

$$\widehat{q_N}(t + \Delta t) = \frac{\Delta t\mathrm{OT}}{1 + \dfrac{\Delta t\nu k^{2n}}{2}} + \left(\frac{1 - \dfrac{\Delta t\nu k^{2n}}{2}}{1 + \dfrac{\Delta t\nu k^{2n}}{2}}\right)\widehat{q_N}(t). \tag{A4}$$

Unless Δt is very small, as $k \to \infty$, the coefficient of $\widehat{q_N}(t)$ asymptotically approaches -1. However, in the absence of OT, the solution of (A2) is

$$\widehat{q_N}(t + \Delta t) = e^{-\nu k^{2n}\Delta t}\widehat{q_N}(t). \tag{A5}$$

Here, for large k and finite Δt, the coefficient of $\widehat{q_N}(t)$ asymptotically approaches zero. Thus the semi-implicit implementation is not strictly correct. Our alternative scheme begins with the equation

$$\frac{\partial}{\partial t}(e^{\nu k^{2n}t}\widehat{q_N}) = e^{\nu k^{2n}t}\mathrm{OT}. \tag{A6}$$

Implementation in the Adams–Bashforth time-stepping scheme is as follows:

$$\widehat{q_N}(t + \Delta t) = e^{-\gamma\Delta t}[\widehat{q_N}(t) + dt_0\mathrm{OT}(t) + dt_1\mathrm{OT}(t - \Delta t)e^{-\gamma\Delta t} + dt_2\mathrm{OT}(t - 2\Delta t)e^{-2\gamma\Delta t}], \tag{A7}$$

where $\gamma = \nu k^{2n}$, $dt_0 = 23\Delta t/12$, $dt_1 = -16\Delta t/12$, and $dt_2 = 5\Delta t/12$. This is equivalent to the direct evaluation of (A2), unlike the semi-implicit scheme, but avoids the frictional limits on the time step imposed by an explicit scheme for (A2).

REFERENCES

Arbic, B. K., 2000: Generation of mid-ocean eddies: The local baroclinic instability hypothesis. Ph.D. dissertation, Massachusetts Institute of Technology–Woods Hole Oceanographic Institution Joint Program, 290 pp.

——, and G. R. Flierl, 2003: Coherent vortices and kinetic energy ribbons in asymptotic, quasi two-dimensional *f*-plane turbulence. *Phys. Fluids,* **15,** 2177–2189.

Batchelor, G. K., 1953: *The Theory of Homogeneous Turbulence.* Cambridge University Press, 121 pp.

Brands, H., J. Stulemeyer, R. A. Pasmanter, and T. J. Schep, 1997: A mean field prediction of the asymptotic state of decaying 2D turbulence. *Phys. Fluids,* **9,** 2815–2817.

Bretherton, F. B., and D. B. Haidvogel, 1976: Two-dimensional turbulence over topography. *J. Fluid Mech.,* **78,** 129–154.

Canuto, C., M. Y. Hussaini, A. Quarteroni, and T. A. Zang, 1988: *Spectral Methods in Fluid Mechanics.* Springer-Verlag, 567 pp.

Charney, J. G., 1971: Geostrophic turbulence. *J. Atmos. Sci.,* **28,** 1087–1095.

——, and M. E. Stern, 1962: On the stability of internal baroclinic jets in a rotating atmosphere. *J. Atmos. Sci.,* **19,** 159–172.

——, and G. R. Flierl, 1981: Oceanic analogues of large-scale atmospheric motions. *Evolution of Physical Oceanography,* B. A. Warren and C. Wunsch, Eds., The MIT Press, 504–548.

Chester, D., P. Malanotte-Rizzoli, J. Lynch, and C. Wunsch, 1994: The eddy radiation field of the Gulf Stream as measured by ocean acoustic tomography. *Geophys. Res. Lett.,* **21,** 181–184.

Dubus, L., 1999: Baroclinic instability of the northeast Atlantic midlatitude meridional currents—Impacts on the large-scale circulation and associated tracer mixing (in French). Ph.D. dissertation, Université de Bretagne Occidentale, Brest, France, 193 pp.

Fine, K. S., A. C. Cass, and W. G. Flynn, 1995: Relaxation of 2D turbulence to vortex crystals. *Phys. Rev. Lett.,* **75,** 3277–3280.

Fjortoft, R., 1953: On the changes in the spectral distributions of kinetic energy for two-dimensional non-divergent flow. *Tellus,* **5,** 225–230.

Flierl, G. R., 1994: Semicoherent oceanic features. *Chaos,* **4,** 355–367.

——, V. D. Larichev, J. C. McWilliams, and G. M. Reznik, 1980: The dynamics of baroclinic and barotropic solitary eddies. *Dyn. Atmos. Oceans,* **5,** 1–41.

Frankignoul, C., and P. Müller, 1979: Quasi-geostrophic response of an infinite beta-plane ocean to stochastic forcing by the atmosphere. *J. Phys. Oceanogr.,* **9,** 104–127.

Fu, L.-L., and G. R. Flierl, 1980: Nonlinear energy and enstrophy transfers in a realistically stratified ocean. *Dyn. Atmos. Oceans,* **4,** 219–246.

Gill, A. E., J. S. A. Green, and A. Simmons, 1974: Energy partition in the large-scale ocean circulation and the production of mid-ocean eddies. *Deep-Sea Res.,* **21,** 499–528.

Hakim, G. J., C. Snyder, and D. J. Muraki, 2002: A new surface model for cyclone–anticyclone asymmetry. *J. Atmos. Sci.,* **59,** 2405–2420.

Held, I. M., and V. D. Larichev, 1996: A scaling theory for horizontally homogeneous, baroclinically unstable flow on a beta plane. *J. Atmos. Sci.,* **53,** 946–952.

Holopainen, E. O., 1961: On the effect of friction in baroclinic waves. *Tellus,* **13,** 363–367.

Hua, B. L., and D. B. Haidvogel, 1986: Numerical simulations of the vertical structure of quasi-geostrophic turbulence. *J. Atmos. Sci.,* **43,** 2923–2936.

Jin, D. Z., and D. H. E. Dubin, 2000: Characteristics of two-dimensional turbulence that self-organizes into vortex crystals. *Phys. Rev. Lett.,* **84,** 1443–1446.

Kamenkovich, I. V., and J. Pedlosky, 1996: Radiating instability of nonzonal ocean currents. *J. Phys. Oceanogr.,* **26,** 622–643.

Keffer, T., 1985: The ventilation of the world's oceans: Maps of the potential vorticity field. *J. Phys. Oceanogr.,* **15,** 509–523.

Kukharkin, N., S. A. Orszag, and V. Yakhot, 1995: Quasicrystallization of vortices in drift-wave turbulence. *Phys. Rev. Lett.,* **75,** 2486–2489.

LaCasce, J. H., 1996: Baroclinic vortices over a sloping bottom. Ph.D. dissertation, Massachusetts Institute of Technology–Woods Hole Oceanographic Institution Joint Program, 220 pp.

Larichev, V. D., and G. M. Reznik, 1976: Two-dimensional Rossby soliton: An exact solution. *Rep. U.S.S.R. Acad. Sci.,* **231** (5); also *POLYMODE News,* No. 19, 3, 6, 12.

——, and I. M. Held, 1995: Eddy amplitudes and fluxes in a homogeneous model of fully developed baroclinic instability. *J. Phys. Oceanogr.,* **25,** 2285–2297.

Lee, S., and I. M. Held, 1991: Subcritical instability and hysteresis in a two-layer model. *J. Atmos. Sci.,* **48,** 1071–1077.

Lorenz, E. N., 1972: Barotropic instability of Rossby wave motion. *J. Atmos. Sci.,* **29,** 259–264.
Mak, M.-K., 1975: The monsoonal mid-tropospheric cyclogenesis. *J. Atmos. Sci.,* **32,** 2246–2253.
Maltrud, M. E., and G. K. Vallis, 1991: Energy spectra and coherent structures in forced two-dimensional and beta-plane turbulence. *J. Fluid Mech.,* **228,** 321–342.
McWilliams, J. C., 1984: The emergence of isolated coherent vortices in turbulent flow. *J. Fluid Mech.,* **146,** 21–43.
——, and G. R. Flierl, 1979: On the evolution of isolated, nonlinear vortices. *J. Phys. Oceanogr.,* **9,** 1155–1182.
——, J. B. Weiss, and I. Yavneh, 1994: Anisotropy and coherent vortex structures in planetary turbulence. *Science,* **264,** 410–413.
Mied, R. D., 1978: The instabilities of finite amplitude barotropic Rossby waves. *J. Fluid Mech.,* **86,** 225–246.
Montgomery, D., W. Matthaeus, W. Stibling, D. Martinez, and S. Oughton, 1992: Relaxation in two dimensions and the sinh–Poisson equation. *Phys. Fluids,* **A4,** 3–6.
Müller, P., and C. Frankignoul, 1981: Direct atmospheric forcing of geostrophic eddies. *J. Phys. Oceanogr.,* **11,** 287–308.
Müller, T. J., and G. Siedler, 1992: Multi-year current time series in the eastern North Atlantic Ocean. *J. Mar. Res.,* **50,** 63–98.
O'Dwyer, J. O., and R. G. Williams, 1997: The climatological distribution of potential vorticity over the abyssal ocean. *J. Phys. Oceanogr.,* **27,** 2488–2506.
Orlanski, I., and M. D. Cox, 1973: Baroclinic instability in ocean currents. *Geophys. Fluid Dyn.,* **4,** 297–332.
Panetta, R. L., 1993: Zonal jets in wide baroclinically unstable regions: Persistence and scale selection. *J. Atmos. Sci.,* **50,** 2073–2106.
——, 1997: Flow organization in regimes of non-parallel baroclinic and barotropic PV gradients. Preprints, *11th Conf. on Atmospheric and Oceanic Fluid Dynamics,* Tacoma, WA, Amer. Meteor. Soc., 311.
Pedlosky, J., 1970: Finite amplitude baroclinic waves. *J. Atmos. Sci.,* **27,** 15–30.
——, 1987: *Geophysical Fluid Dynamics.* 2d ed. Springer-Verlag, 710 pp.
Polvani, L. M., J. C. McWilliams, M. A. Spall, and R. Ford, 1994: The coherent structures of shallow-water turbulence: Deformation radius effects, cyclone/anticyclone asymmetry and gravity-wave generation. *Chaos,* **4,** 177–186.
Rhines, P. B., 1975: Waves and turbulence on a beta plane. *J. Fluid Mech.,* **69,** 417–443.
——, 1977: The dynamics of unsteady currents. *The Sea,* E. D. Goldberg et al., Eds., Marine Modeling, Vol. 6, John Wiley and Sons, 189–318.
——, and W. R. Young, 1982: Homogenization of potential vorticity in planetary gyres. *J. Fluid Mech.,* **122,** 347–367.
Richardson, P. L., 1983: Gulf Stream rings. *Eddies in Marine Science,* A. R. Robinson, Ed., Springer-Verlag, 19–45.
Riviere, P., and P. Klein, 1997: Effects of asymmetric friction on the nonlinear equilibration of a baroclinic system. *J. Atmos. Sci.,* **54,** 1610–1627.
Robinson, A. R., and J. C. McWilliams, 1974: The baroclinic instability of the open ocean. *J. Phys. Oceanogr.,* **4,** 281–294.
Salmon, R., 1978: Two-layer quasi-geostrophic turbulence in a simple special case. *Geophys. Astrophys. Fluid Dyn.,* **10,** 25–52.
——, 1980: Baroclinic instability and geostrophic turbulence. *Geophys. Astrophys. Fluid Dyn.,* **15,** 167–211.
Schecter, D. A., D. H. E. Dubin, K. S. Fine, and C. F. Driscoll, 1999: Vortex crystals from 2D Euler flow: Experiment and simulation. *Phys. Fluids,* **11,** 905–914.
Smith, K. S., and G. K. Vallis, 2001: The scales and equilibration of midocean eddies: Freely evolving flow. *J. Phys. Oceanogr.,* **31,** 554–571.
——, and ——, 2002: The scales and equilibration of midocean eddies: Forced-dissipated flow. *J. Phys. Oceanogr.,* **32,** 1699–1720.
——, G. Boccaletti, C. C. Henning, I. N. Marinov, C. Y. Tam, I. M. Held, and G. K. Vallis, 2002: Turbulent diffusion in the geostrophic inverse cascade. *J. Fluid Mech.,* **469,** 13–48.
Spall, M. A., 2000: Generation of strong mesoscale eddies by weak ocean gyres. *J. Mar. Res.,* **58,** 97–116.
Stammer, D., 1997: Global characteristics of ocean variability estimated from regional TOPEX/Poseidon altimeter measurements. *J. Phys. Oceanogr.,* **27,** 1743–1769.
Stern, M. E., 1975: Minimal properties of planetary eddies. *J. Mar. Res.,* **33,** 1–13.
Vallis, G. K., and M. E. Maltrud, 1993: Generation of mean flows and jets on a beta plane and over topography. *J. Phys. Oceanogr.,* **23,** 1346–1362.
Weatherly, G. L., and P. J. Martin, 1978: On the structure and dynamics of the oceanic bottom boundary layer. *J. Phys. Oceanogr.,* **8,** 557–570.
Wunsch, C., 1997: The vertical partition of oceanic horizontal kinetic energy. *J. Phys. Oceanogr.,* **27,** 1770–1794.
——, 2001: Ocean observations and the climate forecast problem. *Meteorology at the Millenium,* R. P. Pearce, Ed., Academic Press, 217–224.